Multiclass SVM-Based Automated Diagnosis of Diabetic Retinopathy

Adarsh. P and D. Jeyakumari

Abstract— **Diabetes related eye disease is growing as a major health concern worldwide. Diabetic retinopathy is an infirmity due to higher level of glucose in the retinal capillaries, resulting in cloudy vision and blindness eventually. With regular screening, pathology can be detected in the instigating stage and if intervened with in time medication could prevent further deterioration. This paper develops an automated diagnosis system to recognize retinal blood vessels, and pathologies, such as exudates and microaneurysms together with certain texture properties using image processing techniques. These anatomical and texture features are then fed into a multiclass support vector machine (SVM) for classifying it into normal, mild, moderate, severe and proliferative categories. Advantages include, it processes quickly a large collection of fundus images obtained from mass screening which lessens cost and increases efficiency for ophthalmologists. Our method was evaluated on two publicly available databases and got encouraging results with a state of the art in this area**

Index Terms—**Diabetic retinopathy, retinal vessel extraction, exudates, microaneurysms, multiclass SVM.**

I. Introduction

VASCULAR anomalies in the microvasculature of retina due to complication of diabetes are called diabetic retinopathy (DR). Due to high prevalence of retinopathy one out of every five diabetics with newly diagnosed diabetes will also show symptoms of retinopathy. DR is of two type- Type 1 and Type 2 where in India a rampant rise in Type 2 diabetes was reported by World Health Organization (WHO) [1]. The premature signs of retinal degeneration arise from capillary wall breakdown, seen on the fundus as small red dots called vessel microaneurysms (MAs). Besides this serum lipid leaking from the damaged vessels get precipitated as bright yellow lesions called hard exudates. As a result a white fluffy opaque lesion known as soft exudates or cotton wool spots is formed along the nerve fiber layer. Up to this it is known as non-proliferative diabetic retinopathy (NPDR). Extensive starvation for oxygen due to severe occlusions generates new fragile vessels. This is called proliferative diabetic retinopathy (PDR) which highly threatens visibility [2]. Periodic screening of eye will help in preventing the pathology at an early stage but the process of DR screening system is an arduous effort. Thus, there is surge demand for impeccable medical systems that can screen a collection of images to detect early signs of retinopathy with least expense.

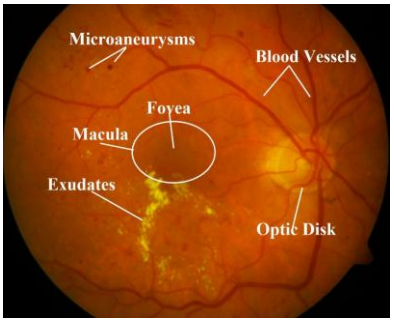

Fig. 1. Sample digital fundus image with DR

All the earlier retinal vessel segmentation methods in fundus images were classified into three- thresholding, tracking and machine trained classifiers [3]-[5]. Chutatape *et al.* [6] identified exudates using a combination of finding seeds, edge detection and region growing. Niemeijer *et al.* [7] distinguished bright lesions from colour retinal images by classifying pixels using a probability map. In [8] presented automated exudates detection based on computational intelligence technique and fuzzy c-means clustering where feature vectors are classified using multilayer neural network. Mizutani *et al.* [9] detected MAs based on double ring filter in non-contrast images of the retinal fundus. Later red dots were detected using mathematical morphological black top hat and their features estimated by SVM classifier [10]. Then a two stage approach was suggested for MA based on Radon transformation without the need of explicit training [11]. Antal *et al.* [12] realized an ensemble-based framework to improve microaneurysm detection using preprocessing methods and candidate extractors.

This paper focuses on the automated detection of DR by extracting features in a fundus using morphological operations. Out of the extracted features, few are selected on the basis of significance test and trained with the multiclass SVM built on one against all approach. Then multiclass SVM organizes the images into normal, mild, moderate, severe and or proliferative categories. Work organized as, Section II describes the feature extraction, feature selection and multiclass SVM classifier.

Adarsh.P is a PG Scholar with Department of Electronics and Communication, RVS College of Engineering and Technology, Coimbatore-641402, Tamilnadu, India (e-mail: adarshp321@gmail.com).

D. Jeyakumari is working as Associate Professor with the Department of Electronics and Communication, RVS College of Engineering and Technology, Coimbatore-641402, Tamilnadu, India (e-mail: dgjeyakumari@gmail.com).

978-1-4673-4866-9/13/$31.00 ©2013 IEEE

Section III presents the experimental results and ROC analysis for performance evaluation, with conclusion in Section IV.

II. PROPOSED METHOD

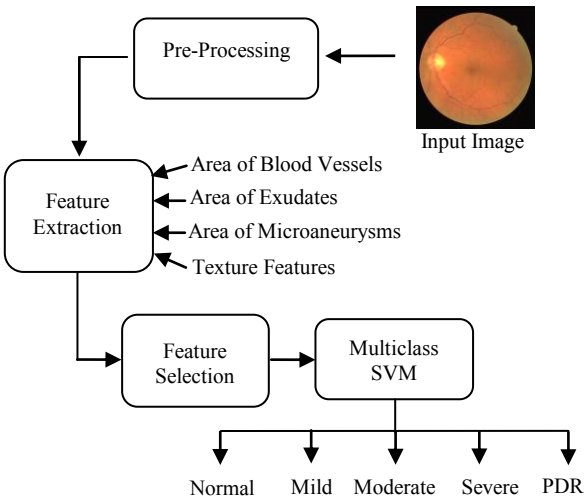

Fig. 2. Block diagram of the automated diagnosis system of DR

A. Pre-Processing

In order to correct aberrations due to uneven illumination pre-processing phase is carried out. From the input color image, the green channel image is preferred for further processes because of its better contrast. The contrast of the fundus image tends to be bright in the centre and diminish at the side, hence preprocessing is essential to minimize this effect and have a more uniform image. After converting the green channel image to grayscale image contrast enhancement is made with the help of contrast limited adaptive histogram equalization (CLAHE).

B. Blood Vessel Detection

Blood vessel extraction is a key process for the identification of DR. Let (I_1) be the one time CLAHE applied image of green channel image of Fig 4(a). We apply the morphological opening operator (Φ) on (I_1) with a ball-shaped structuring element (SE) of fixed radius eight ($B8$) since with disk histogram is not smooth (Eq. (2)) to remove small noise to get the final image (I_2)

$$I_2 = \Phi_{B8}(I_1) \quad (1)$$

Optic disk removed image (I_3) is obtained by subtracting (I_2) from (I_1) i.e. (I_3) = (I_1) - (I_2). Image (I_3) is then binarized by considering 0.10 as threshold which is based on histogram analysis. There may be some noise in the binary image. To reduce the noise connected component analysis is used on (I_3) and finally obtains the blood vessel image (I_4). Fig (1) is once again applied with CLAHE thrice and thresholding to give another blood vessel image (I_5). Meanwhile Fig (1) color fundus image is converted into gray-scale using Craig's formula in Eq. (2). Let I_6 be the transformed grayscale image of Fig 4(a),

$$I_6 = 0.3 \times R + 0.59 \times G + 0.11 \times B \quad (2)$$

Later optic disk is detected by finding the maximum intensity pixels in (I_6). A mask is created around the optic disk and added to (I_5). Radius taken for the mask was 90. After this (I_4) and (I_5) are compared using AND operation and the noises are removed. Final blood vessel image is obtained by removing the circular border which is created using canny edge detection and morphological opening operation.

C. Exudates Detection

As they appear as bright yellow-white deposits on the retina their shape and size will vary with different retinopathy stages. To start exudate detection we start with gray scale image (I_6).To eliminate the blood vessels we apply a gray-scale morphological closing operator (Ψ) on intensity adjusted (I_6) with the similar SE of fixed size radius ten ($B10$) and obtain (I_7) as the final image.

$$(I_7) = \Psi_{B10}(I_6) \quad (3)$$

For closing operation, radius of the SE depends on the maximum radius of the blood vessels. As it has been observed that in most of the fundus images of size 1500 x 1152, the maximum size of the radius is within 10 pixels and it has guided us to. Later exudate area is detected using column wise neighbourhood operation which processes (I_7) by rearranging each M x N block of (I_7) into a column of a temporary matrix (I_8). This operation is performed to remove most of the unwanted artifacts leaving only the border, exudates and the optic disc. In our experiment block size was taken as 6x6. Image (I_8) is then binarized by considering 0.45 as threshold. The region of exudates is detected and after subtracting the border and optical disk to give image (I_9). Then operator (Ψ) is used to expand the exudates region and remove the noise persisting after column filtering, resulting in (I_{10}). On the other side once again (I_6) is applied with CLAHE and non-exudates are identified using threshold value of 0.85 to give (I_{11}). After this (I_{10}) and (I_{11}) are compared using AND operation and to detect the exudates.

D. Microaneurysms Detection

The most challenging part in the DR detection is the isolation of MAs which is done as (I_1) taken and applied with canny edge detection to give image (I_{12}). Later circular border is subtracted from (I_{12}) and background pixel filling is used to obtain (I_{13}) resulting in initial MAs detected image (I_{14}).

$$(I_{14}) = (I_{13}) - (I_{12}) \quad (4)$$

Then remaining large area is found and subtracted from (I_{14}) to exclude the large area noise resulting in (I_{15}). Meanwhile the green channel image is twice contrast enhanced and binarized by considering 0.7 as threshold to give (I_{16}). After this (I_{15}) and (I_{16}) are compared using AND operation to obtain the exudates removed image (I_{17}). The same twice contrast enhanced green channel image is binarized with 0.3 as threshold to give (I_{18}). Then (I_{17}) and (I_{18}) are compared using AND operation to obtain the vasculature removed image (I_{19}). Finally microaneurysms are obtained by subtracting the optical disk.

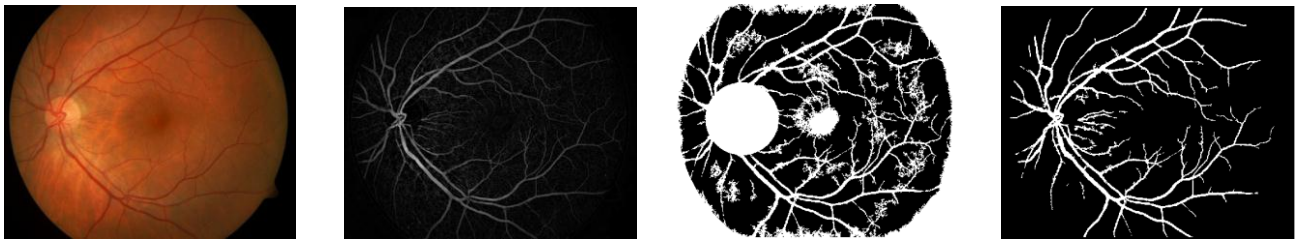

(a) (b) (c) (d)

Fig. 3. Illustration of blood vessel detection (a) Input image. (b) Optic disk removed image. (c) Image with mask after removing noise (d) Final output

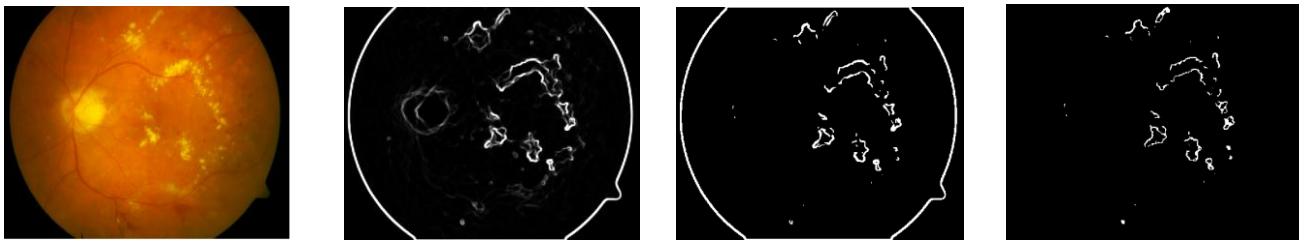

(a) (b) (c) (d)

Fig. 4. Illustration of exudate detection (a) Input image. (b) Intensity adjusted grayscale image.(c) Morphological closing.(d) After column filtering.

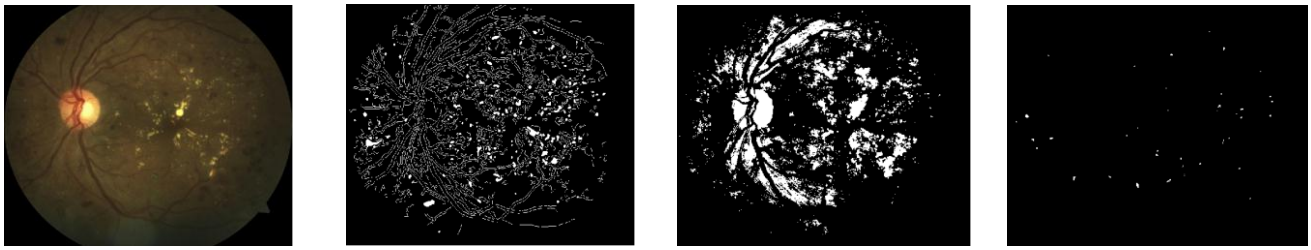

(a) (b) (c) (d)

Fig. 5. Illustration of microaneurysm detection (a) Input image. (b) After column filtering. (c) Region of exudates without optic disk. (d) Final MAs.

E. Feature Extraction

Both anatomical and texture properties of the fundus image were extracted which includes:

1) Area Calculations: The areas of blood vessels, exudates, microaneurysms are obtained by using two loops to count the number of pixels with binary 1 (white) in the final segmented exudate and microaneurysms image.

2) Texture Features: The function of spatial variation in pixel intensities (gray value) is known as image texture. Let z_i denote the values of all possible intensities in an M x N image, where i=0,1,….,L-1. The probability, $p(z_k)$, of intensity level z_k occurring in a input image is specified by

$$p(z_k)= \frac{n_k}{MN} \tag{5}$$

where n_k is the number of times that intensity z_k occurs in the image and MN is the total number of pixels. Once we have $p(z_k)$, the mean intensity is given by

$$m= \sum_{k=0}^{L-1} n_k\, p(z_k) \tag{6}$$

Similarly standard deviation (SD) is a measure of the spread of the values of z about mean, and is given by square root of variance of the intensities,

$$\sigma= \sqrt{\sum_{k=0}^{L-1} (z_k - m)^2\, p(z_k)} \tag{7}$$

Third moment is a measure of the skewness of the histogram. It is given by:

$$\mu_3(z)= \sum_{k=0}^{L-1} (z_k - m)^3\, p(z_k) \tag{8}$$

Entropy is a statistical measure of the disorder or randomness in a grayscale image which is given by:

$$Entropy= -\sum p(z_k) log_2 p(z_k) \tag{10}$$

GLCM is created by calculating how often a pixel with gray level value i occurs in a specific spatial relationship to a pixel with the value j. It returns a value between 0 and 1.

$$Homogeneity = \sum_{i,j} \frac{p(i,j)}{1+|i-j|} \tag{11}$$

Contrast is defined as the local variation in the GLCM. Measurement of the joint probability occurrence of specified pixel pairs is referred as correlation. Energy is mentioned as uniformity or angular second moment and it provides the algebraic sum of squared elements in the GLCM.

F. Feature Selection

Out of 11 features which include three area calculations (blood vessel, exudate, and microaneurysm) and eight texture features in order to choose the significant one among them we have used Anova test. It is a hypothesis test that makes the test statistic to follow a distribution if a null hypothesis is true. Probability value (*p-value*) acquired through this test is used to determine how statistically significant is the set of feature data. Lower the p-value implies that the features data are clinically significant. Thus, the lower the *p-value* (i.e. with $p< 0.05$) the more difference is there between the abnormal and normal set of features data [13]. In this way area of exudates, area of microaneurysms, mean, third moment and entropy are found as statistically significant sets of features for SVM classification.

G. Multiclass SVM Classifier

The basic function of binary SVM is to find the hyper-plane that best separates vectors from both classes in feature space at the same time maximizing the distance from each class to the hyperplane [14]. Let the separating hyperplane be defined by $x.\ w + b = 0$, where w is its normal. For linearly separable data labeled $\{x_i, y_i\}, x_i \in \Re^{N_d}$, $y_i = \{-1,1\}$, $i = 1, .., N$, the optimum boundary chosen with maximal margin criterion is found by minimizing the objective function; $E = \|w\|^2$.

$$(x_i \cdot w + b) y_i \geq 1, \quad \text{for all } i. \tag{12}$$

The solution for the optimum boundary w_0 is a linear combination of a subset of the training data, $s \in \{1 \ldots N\}$: the support vectors. These support vectors define the margin edges and satisfy the equality $(x_s \cdot w_0 + b) y_s = 1$. Data may be classified by computing the sign of $x \cdot w_0 + b$. Generally, the data are not separable and the inequality in equation (7) cannot be satisfied. In this case, a "slack" variable ξ_i that represents the amount by which each point is misclassified is introduced. The new objective function is now reformulated as

$$E = \frac{1}{2}\|w\|^2 + C\sum_{i=1}^{N} L(\xi_i) \tag{13}$$

$$\text{Subject to} \quad (x_i \cdot w + b) y_i \geq 1 - \xi_i \quad \text{for all } i. \tag{14}$$

L is a cost function and C is a hyper-parameter that trades-off the effects of minimizing the empirical risk against maximizing the margin. The first term can be thought of as a regularization term, deriving from maximizing the margin, which gives the SVM its ability to generalize well on sparse training data. To allow for nonlinear decision surfaces, the training data may be projected into a high-dimensional space $\boldsymbol{H}$ through a mapping function ϕ, or ϕ: $\boldsymbol{R}^q \rightarrow \boldsymbol{H}$. An input data point x can be represented as $\phi(x)$ in the high-dimensional space $\boldsymbol{H}$. The expensive computation of $(\boldsymbol{\phi}(x) \cdot \boldsymbol{\phi}(x_i))$ in a high-dimension space is reduced by a positive definite kernel,

$$(\phi(x) \cdot \phi(x_i)) = k(x, x_i) \tag{15}$$

Two main approaches are used for multiclass classification using SVM, "one-against-all" and "one-against-one" [15]. In this paper "one-against-all" approach is implemented with a set of binary classifiers, each of them trained to separate one class from the remaining. This is done by allocating each pixel to the class for which the largest decision value was calculated. With this approach after solving (8), for a case x_i there are q decision functions, where q is the number of classes,

$$(w_i)^{\mathrm{T}} \phi(x) + b_j, \text{ where } j = 1, \ldots, q. \tag{16}$$

For each of the q analyses, this allocation indicates that the particular case is either belongs to class under consideration or try for the rest of classes. The training process analyzes training data to find an optimal way to classify images into their respective classes. Hence the training data set should be statistically significant.

III. Experimental Results

A. Image Acquisition

For this work we have used two publicly available databases. The DIARETDB1 [16] database consists of 89 colour fundus images of which 84 contain at least mild signs of NPDR, and 5 are normal. The DIARETDB0 [17] database consists of 130 color fundus images of which 20 are normal and 110 contain signs of DR. The images were taken in the Kuopio university hospital. Images were captured with 50 degree FOV (field of- view) digital fundus cameras with unknown camera settings. Based on the ground truths provided with the database an image without lesions is considered normal and the one with lesions like exudates, microaneurysms and hemorrhages is considered abnormal which includes mild, moderate, severe and proliferative DR.

B. Performance Evaluation

Two databases were manually assigned into categories representing the progressive states of retinopathy: normal, mild, moderate and severe non-proliferative, and proliferative. The images of DIARETDB1 were divided into training (28 images) and test sets (61 images); whereas the images of DIARETDB0 were divided into training (42 images) and test sets (88 images). After training the multiclass SVM classifier with the training data set, entire algorithm was run on two datasets using a PC with an Intel i3 Processor and 2 GB RAM. The average run time of MATLAB code for an image was found to be 15 seconds. To evaluate the system; performance metrics such as sensitivity, specificity and accuracy are calculated. The equations are given below:

$$\bullet \text{Sensitivity}(\%) = \frac{\mathrm{TP}}{\mathrm{TP}+\mathrm{FN}} \times 100\% \tag{17}$$

$$\bullet \text{Specificity}(\%) = \frac{\mathrm{TN}}{\mathrm{TN}+\mathrm{FP}} \times 100\% \tag{18}$$

$$\bullet \text{Accuracy}(\%) = \frac{\mathrm{TP}+\mathrm{TN}}{\mathrm{N}} \times 100\% \tag{19}$$

The terms used to measure the test performance are true positive (TP), true negative (TN), false positive (FP), false negative (FN) and total number of images (N). Results obtained for each test set are given in Table I.

TABLE I
COMPARISON OF THE PERFORMANCE MEASURES OF THE DATASETS

Source	Sensitivity (%)	Specificity (%)	Accuracy (%)
DIARETDB0	90	94.3	96
DIARETDB1	91.2	93	94.6
Average	90.6	93.65	95.3

C. *Receiver Operating Characteristics (ROC)*

The classification effectiveness was also analyzed with the help of receiver operating characteristic (ROC) curves. ROC curves are plotted; sensitivity (true positive rate) versus 1-specificity (false positive rate) for varying thresholds on the posterior probabilities. A pair formed by sensitivity and 1-specificity value is plotted as a graph for each threshold value resulting in a curve as shown in Fig. 6. If an ROC curve approaches closer to the top left corner, the better will be the performance of the method. Area under the ROC curve (AUC) implies the classifier's performance within the entire range of cut-off points. A system that agrees completely with the ground truth segmentations would yield an area under ROC curve A_z= 1. The AUC value obtained here is above 0.96 which displays the classifier performance is excellent.

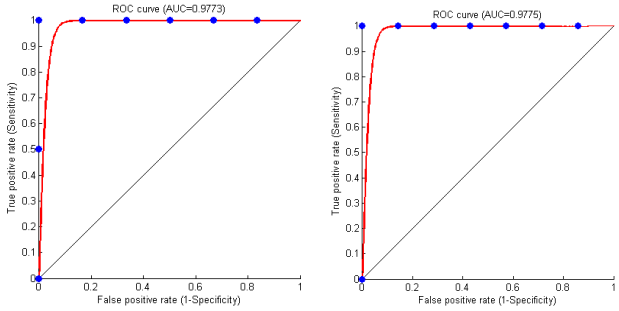

(a) (b)

Fig. 6.ROC curve for (a) Microaneurysm and (b) Exudates classifications

IV. CONCLUSION

Assessment of the proposed method with earlier approaches mentioned in the literature is given in Table II. Information from the segmentation is integrated through the use of the supervised classifier presented. The multiclass SVM classifier has a computationally challenging training phase, but assures a swift classification phase and good performance. Furthermore, the work presented is conceptually simple and efficiently implementable. We have performed experiments training the classifier with each of the DIARETDB1 and DIARETDB0 databases while testing it on the other. The results obtained are really encouraging and with respect to ROC analysis. To synopsize, we have developed and evaluated an effectual computer-aided diagnosis system that takes into account anomalies of multiple forms and provides an unswerving analysis as human observers are subjective and susceptible to faults.

TABLE II
COMPARISON OF RESULTS WITH PREVIOUS METHODS

Author	Number of Images	Sensitivity (%)	Specificity (%)
Sinthaniyothin	30	88.5	99.7
Chutatape	35	100	71.0
Wang *et al.*	154	100	70.0
Proposed Method	219	90.6	93.6

REFERENCES

[1] M. Rema and R. Pradeepa, "Diabetic retinopathy: An Indian perspective", *Indian J Med Res* 125, March 2007, pp. 297-310..

[2] Luca Giancardo, "Automated Fundus Images Analysis Techniques to Screen Retinal Diseases in Diabetic Patients", PhD Thesis, University of Bourgogne, France, 27 September 2011.

[3] Xu Y, Zhang H, Li H and Hu GS: "An improced algorithm for vessel centerline tracking in coronary angiograms". *Comput Meth Prog Bio* 2007, 88:131-143.

[4] Joao VBS, Jorge JGL, Roberto MCJ, Herbert FJ and Michael JC, "Retinal Vessel Segmentation Using the 2-D Gabor Wavelet and Supervised Classification". *IEEE Trans Medical imaging* 2006, 25:1214-1222.

[5] C. Sinthanayothin, J. F. Boyce, T. H. Williamson, H. L. Cook, E. Mensah, S. Lal, D. Usher. "Automated detection of diabetic retinopathy on digital fundus images". *Diabetic Medicine*, 19:105–112, 2002.

[6] H. Li and O. Chutatape, "A model based approach for automated feature extraction in fundus images," *Proc. 9th IEEE International Conference on Computer Vision*, Nice, France, October 2003.

[7] Niemeijer.M, Abramoff.M.D and Van Ginneken.B, "Information fusion for Diabetic Retinopathy CAD in Digital color fundus photographs" *IEEE Transactions on Medical Imaging*, vol. 26, no. 10,pp. 1357-1365, October, 2007.

[8] Alireza Osareh, Bita Shadgar, and Richard Markham: "A Computational-Intelligence-Based Approach for Detection of Exudates in Diabetic Retinopathy Images" *IEEE Transactions on Information Technology in Biomedicine*, vol. 13, no. 4, pp.535-545, July 2009.

[9] A. Mizutani, C. Muramatsu, Y. Hatanaka, S. Suemori, T. Hara and H. Fujita, "Automated microaneurysm detection method based on double ring filter in retinal fundus images," *Proc. SPIE*, vol. 7260, pp. 72601 N-1-8, Feb. 2009.

[10] L. Xu and S. Luo, "Optimal algorithm for automatic detection of microaneurysms based on receiver operating characteristic curve," *J. Biomedical Optics*, vol. 15, no. 6, pp. 065004-1-6, Dec. 2010.

[11] L. Giancardo, F. Meriaudeau, T. P. Karnowski, K. W. Tobin,Y. Li, and E. Chaum, "Microaneurysms Detection with the Radon Cliff Operator in Retinal Fundus Images," *SPIE Medical Imaging*, vol. 7623, pp. 29, 2010.

[12] B. Antal, and A. Hadju, " An Ensemble-Based System for Microaneurysm Detection and Diabetic Retinopathy Grading," *IEEE Transactions On Biomedical Engineering,* vol. 59, No. 6, June 2012.

[13] "ANOVA," www.physics.csbsju.edu/stats/**anova**.html

[14] V. Vapnik, *Statistical Learning Theory*, New York: Willey, 1998.

[15] G. H. Halldorsson, J. A. Benediktsson, and J. R. Sveinsson, "Support vector machines in multisource classification," in *Proc. IGARSS*, Toulouse, France, Jul. 21–25, 2003, pp. 2054–2056.

[16] "DIARETDB1 - Standard Diabetic Retinopathy Database," http://www2.it.lut.fi/project/imageret/diaretdb1/index.html

[17] "DIARETDB0 - Standard Diabetic Retinopathy Database," http://www2.it.lut.fi/project/imageret/diaretdb0/index.html